PHYSICAL REVIEW E **68**, 060301(R) (2003)

Projectile-shape dependence of impact craters in loose granular media

K. A. Newhall and D. J. Durian
Department of Physics & Astronomy, UCLA, Los Angeles, California 90095-1547, USA
(Received 9 September 2003; published 24 December 2003)

We report on the penetration of cylindrical projectiles dropped from rest into a dry, noncohesive granular medium. The cylinder length, diameter, density, and tip shape are all explicitly varied. For deep penetrations, as compared to the cylinder diameter, the data collapse onto a single scaling law that varies as the 1/3 power of the total drop distance, the 1/2 power of cylinder length, and the 1/6 power of cylinder diameter. For shallow penetrations, the projectile shape plays a crucial role with sharper objects penetrating deeper.

DOI: 10.1103/PhysRevE.68.060301 PACS number(s): 45.70.Cc, 83.80.Fg

Anyone who has walked across a beach realizes that even though the sand moves under the pressure of a step, at some point their foot is supported. Someone who is running leaves a deeper and larger footprint, or crater, than someone who is walking. This phenomenon applies to anything dropped into sand; no matter how energetic the impact, the sand will eventually stop the projectile. For an object of mass m that is dropped from rest and that moves downwards a total distance H (including motion throughout the impact), the gravitational potential energy mgH is transfered from the projectile to the sand. Some of this energy is dissipated and some of it is converted back to gravitational potential energy associated with the size and shape of the crater. Fundamentally, the energy is expended by an average stopping force $\langle F \rangle$ applied by the sand as the projectile moves a total distance d from initial impact to rest:

$$\langle F \rangle d = mgH. \tag{1}$$

Thus, a straightforward measurement of d vs H provides information about granular mechanics, a topic of widespread interest [1,2]. A full understanding of the stopping forces and the transfer of energy may enable a fundamental explanation for such impact-related phenomena as the complex sequence of crater morphologies [3–6] and the spectactular granular jets formed by a collapsing hole [7,8].

The penetration of spheres into loose granular media has been reported previously. In Ref. [9], the total drop distance H was varied by up to a factor of 1000; the projectile density ρ_p was varied by a factor of 60; the projectile diameter D_p was varied by a factor of 4; the grain density ρ_g was varied by a factor of 2; and the tangent of the draining repose angle μ was varied by a factor of 2. The resulting penetration depths are reproduced in Fig. 1, along with the observed scaling law

$$d = 0.14\left[\left(\frac{\rho_p}{\rho_g \mu^2}\right)^{3/2} D_p^2 H\right]^{1/3}. \tag{2}$$

From the combined dependence on projectile density and drop height, $(\rho_p H^{2/3})^{1/2}$, we note that the penetration depth is not a function of either the sphere's kinetic energy, $\sim \rho_p H$, or its momentum, $\sim \rho_p H^{1/2}$, at impact. In Ref. [6] a different definition of crater depth, suitable when the spheres completely submerge, gave a different scaling.

The behavior in Fig. 1 cannot be explained by current theories. Granular hydrodynamics and a rate-independent ''plowing'' force both predict different scaling than Eq. (2) (see discussion in Ref. [9]). But how general is the observation? In particular, how does the crater depth depend upon the shape of the projectile? One would expect a pointed projectile to penetrate deeper than a blunt projectile. Perhaps this may be accounted for by the value of the numerical coefficient in Eq. (2). Or perhaps the functional form of depth vs drop distance may be entirely different, with $d \sim H^{1/3}$ arising as an accident of the projectile's spherical shape.

To explore the role of projectile shape on impact cratering, we perform a series of experiments with the same basic protocol as in Ref. [9]. Namely, we fill a 1000 ml beaker (diameter 4 in.) with dry, noncohesive glass beads (diameter 0.2 mm, draining respose angle 24°). The depth of filling is 2 in. for most trials, but is increased to 4 in. for deep impacts. The density of the granular medium is $\rho_g = 1.51$ g/cc, which corresponds to random-close packing with a volume fraction of about 63%. As in Ref. [9], this state is achieved by swirling the sample horizontally, at first rapidly and then ever more slowly, until the surface is level and at rest. Instead of dropping spheres, we now drop a wide variety of cylinders and measure their depth of penetration. Cylinder materials include wood (poplar, $\rho_p = 0.5$ g/cc), aluminum (Al, $\rho_p = 2.7$ g/cc), and high-density tungsten carbide (WC, $\rho_p = 17.1$ g/cc). We use four different cylinder diameters, $D_p \in \{0.25$ in., 0.50 in., 1.0 in., 2.0 in.$\}$, and four different cylinder lengths, $L \in \{0.5$ in., 1 in., 2 in., 4 in.$\}$. To vary the projectile shape, progressively sharper conical tips are machined at one end of these cylinders; we use four different

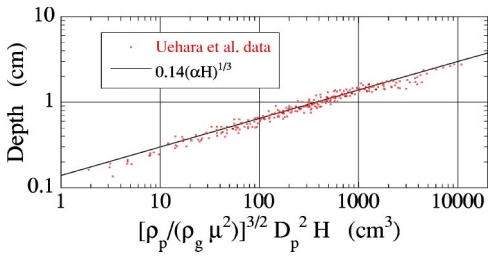

FIG. 1. Crater depth vs scaled total drop distance. All data are from Ref. [9] for spherical projectiles. The solid line is the power-law scaling given by Eq. (2).

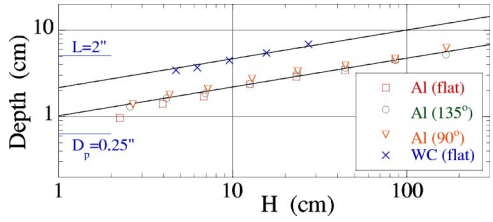

FIG. 2. Crater depth vs drop distance for four different cylindrical projectiles, all with diameter $D_p = 0.25$ in. and length $L = 2$ in. The solid lines represent fits to a 1/3 power law, $d \sim H^{1/3}$.

cone angles, {180° (i.e., flat), 135°, 90°, 45°}. To achieve a vertical orientation at impact, the cylinders are suspended by a thin loop of thread, tied through an accurately machined hole. For each cylinder, the drop distances are varied as widely as possible within certain limitations. The minimum is set either by the penetration depth for a cylinder placed infinitesimally above the surface of the medium or by the tendency of (long or light) cylinders to tip over after a shallow penetration. The maximum drop distance is set either by the depth of the sand or by the tendency of cylinders to begin to tumble during free fall. No trial is accepted unless the cylinder remains vertical after impact.

Four sets of penetration depth vs drop distance data are displayed in Fig. 2, all for cylindrical projectiles of length 2 in. and diameter 0.25 in. This includes WC and Al rods with flat ends, as well as Al rods with 135° and 90° tips. Evidently WC penetrates deeper than Al, in accord with their densities. The three Al rods all penetrate to approximately the same depth, in spite of their different tip shapes. Furthermore, all data are adequately described by a 1/3 power law, $d \sim H^{1/3}$, just as for spherical projectiles. Therefore, the projectile shape seems to play no crucial role and the prior scaling law is not special to spheres.

The results in Fig. 2 severely constrain the generalization of Eq. (2) to aspherical projectiles. A natural hypothesis is that the crucial parameter is the mass per unit cross sectional area, $(2/3)\rho_p D_p$ for spheres and $\rho_p L$ for cylinders. For cylinders, equal variation of density and length should lead to equal variation of penetration depth. Thus, we must have

$$d = 0.14\left[\left(\frac{\rho_p L}{\rho_g \mu^2}\right)^{3/2} D_p{}^{1/2} H\right]^{1/3} \qquad (3)$$

for consistency with Eq. (2).

To test this expectation, we display depth data vs scaled drop height, $[(\rho_p L)/(\rho_g \mu^2)]^{3/2} D_p{}^{1/2} H$, in Figs. 3(a)–3(d). This allows us to plot Eq. (3) as a single curve, onto which we look for all data to collapse. Each subplot is for a different rod diameter; symbol types distinguish rods according to their length, density, and tip shape. Evidently, the degree of collapse is better for deeper penetrations and is worse for shallower penetrations. In Fig. 3(a), for the 0.25 in. diameters, the quality of collapse is comparable to that found earlier for spheres. Comparison of the four subplots shows that the onset of collapse appears correlated with rod diameter. In particular, collapse by Eq. (3) seems to be attained when the penetration is larger than the rod diameter. For

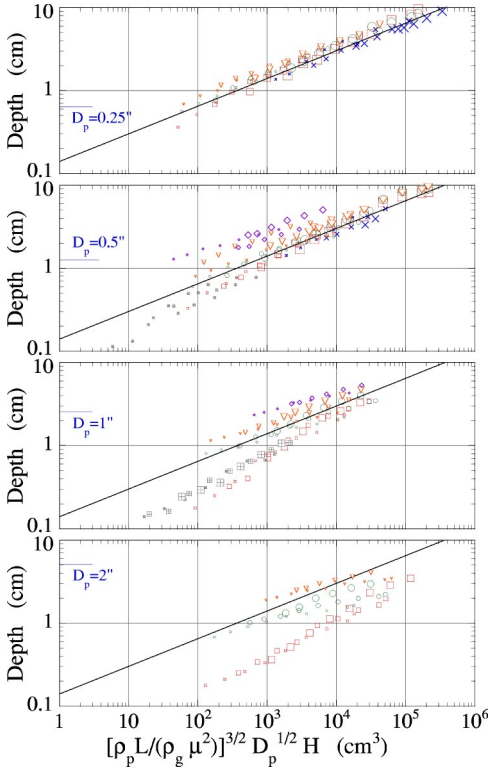

FIG. 3. Crater depth vs scaled total drop distance. Data are for cylindrical objects, divided into graphs by cylinder diameter, as labeled. Values of L varied from 0.5 in., indicated by the smallest symbols, to 1.0 in., to 2.0 in., to 4 in. by larger symbols. Tungsten carbide is denoted by ×, flat-ended aluminum by □, 135°-tip aluminum by ○, 90°-tip aluminum by ▽, 45°-tip aluminum by ◇ and flat-ended wood by □. The line in each subplot is Eq. (3).

shallower penetration, Eq. (3) fails and the actual depth depends on tip shape. In this regime, sharper tips cause deeper penetration. The tendency of the data to deviate from $d \sim H^{1/3}$ for small H, concomitant with the onset of shape dependence, can also be seen in close reinspection of Fig. 2.

In conclusion, the crater depth vs drop height scaling observed previously for spheres is robust and can be simply generalized to projectiles of different shapes. The $d \sim H^{1/3}$ power law is not an accident of projectile shape. The only accident is that it holds for spheres even when the penetration is not greater than the sphere diameter. The independence of deep penetrations on projectile shape, as observed here, should heighten the importance of finding a full theoretical understanding. It also offers a clue: The dissipation of the projectile's energy in the granular medium must occur throughout a volume that is much larger than the crater. Presumably, this involves a cooperative effect of many grains, such as long force chains successively created then broken by the projectile impact. The finite size of the granular sample should then play a role, especially for deeper penetrations, and this could be tested experimentally. So far, we have only ensured that the sample is sufficiently deep as to not affect the penetration depths.

To bring this manuscript full circle, we return to a walk on the beach. In particular, we generalize the depth scaling law to projectiles with noncircular cross section and we predict

the depth of footprints in dry noncohesive sand [$\rho_g = 1.59$ g/cc, $\mu = \tan(38°)$ [9]]. Making three substitutions, $\rho_p L$ with the mass per cross sectional area m/A, D_p with $2\sqrt{A/\pi}$, and H with $v^2/(2g)$, we arrive at

$$d = 0.11\left(\frac{m/A^{3/2}}{\rho_g \mu^2}\right)^{1/2}\left(\frac{Av^2}{g}\right)^{1/3}. \quad (4)$$

The area factors have been distributed to make more apparent that this expresssion is dimensionally correct; at constant mass, the depth decreases with area as $d \sim A^{-5/12}$. For impact by a foot, we take $A = 8 \times 30$ cm^2, $m = 70{,}000$ g, and $v = 100$ cm/s (corresponding to a drop height of 5 cm). For these numbers Eq. (4) predicts a footprint depth of 6.7 cm, in reasonable accord with experience.

We thank Françoise Queval for coordinating the ''Research Experience for Undergraduates'' program at UCLA; we thank John de Bruyn and Lev Tsimring for useful discussions. This material is based upon work supported by the National Science Foundation under Grant Nos. DMR-0305106 and PHY-0243625.

[1] H.M. Jaeger, S.R. Nagel, and R.P. Behringer, Rev. Mod. Phys. **68**, 1259 (1996).

[2] J. Duran, *Sands, Powders, and Grains: An Introduction to the Physics of Granular Materials* (Springer, New York, 2000).

[3] *Impact and Explosion Cratering*, edited by D.J. Roddy, R.O. Pepin, and R.B. Merril (Pergamon Press, New York, 1978).

[4] H.J. Melosh, *Impact Cratering: A Geologic Process* (Oxford University Press, New York, 1989).

[5] K. Holsapple, Annu. Rev. Earth Planet Sci. **21**, 333 (1993).

[6] A.M. Walsh, K.E. Holloway, P. Habdas, and J.R. de Bruyn, Phys. Rev. Lett. **91**, 104301 (2003).

[7] S. Thoroddsen and A. Shen, Phys. Fluids **13**, 4 (2001).

[8] R. Mikkelsen, M. Versluis, E. Koene, G.-W. Bruggert, D. van der Meer, L. van der Weele, and D. Lohse, Phys. Fluids **14**, S14 (2002).

[9] J.S. Uehara, M.A. Ambroso, R.P. Ojha, and D.J. Durian, Phys. Rev. Lett. **90**, 194301 (2003).